Physics Letters A 376 (2011) 24–30

Contents lists available at SciVerse ScienceDirect

Physics Letters A

www.elsevier.com/locate/pla

Collisional effects in the tokamap

A.B. Schelin [a], I.L. Caldas [b], R.L. Viana [c,*], S. Benkadda [d]

[a] Departamento de Física, Universidade Tecnológica Federal do Paraná, 80230-901, Curitiba, Paraná, Brazil
[b] Instituto de Física, Universidade de São Paulo, 5315-970, São Paulo, São Paulo, Brazil
[c] Departamento de Física, Universidade Federal do Paraná, 81531-990, Curitiba, Paraná, Brazil
[d] International Institute for Fusion Science, CNRS-Université de Provence, Centre de St. Jérôme, Case 321, 13397 Marseille, France

ARTICLE INFO

Article history:
Received 28 July 2011
Received in revised form 28 September 2011
Accepted 17 October 2011
Available online 21 October 2011
Communicated by F. Porcelli

Keywords:
Symplectic maps
Chaotic magnetic field lines
Tokamap

ABSTRACT

Plasmas confined in tokamaks with non-symmetric perturbations are surrounded by a chaotic layer of magnetic field lines that guide charged particles to the tokamak wall. We use an analytical two-dimensional symplectic mapping to study the resulting fractal patterns of field line escape. However, particles may experience several collisions before escaping toward the tokamaks wall. We add a random collisional term to the field line mapping to investigate how the particle collisions modify their escape patterns.

1. Introduction

There has been a growing recognition that the nonlinear dynamics of magnetic field lines plays an important role in tokamak plasmas [1]. One of the distinctive features of this nonlinearity is the possibility of chaotic behavior of magnetic field lines [2]. Here, chaos refers to the Lagrangian description of the field lines structure, which is time-independent [3]. Chaotic behavior of magnetic field lines is found not only to be typical but also desirable, when the problem of particle and heat deposition on the tokamak wall is considered. The main purpose behind the creation of a chaotic zone is to obtain a uniform – and therefore cold – distribution of escaping field lines and particles [4–6]. Recent studies, however, have shown that in many situations this is not the case [7,9,10]. Rather, the chaotic dynamics creates a non-uniform distribution pattern as a consequence of the presence of chaotic sets in the chaotic zone [11].

Geometrically, these sets form a fractal structure, since their underlying structure is the homoclinic intersection of invariant manifolds of fixed points embedded in the chaotic region [7,9,12]. The magnetic field lines in a toroidal confinement scheme like a tokamak represent a Hamiltonian system, where the toroidal coordinate plays the role of time, and the remaining coordinates stand for the canonically conjugated variables [1]. The magnetic line flow in the presence of "time"-dependent perturbations (necessary to bring about chaotic motion) has no fixed points. However, in the description we adopt in our Letter we investigate a Poincaré map of the magnetic field line flow. Since this map is "time"-independent by construction (its equations do not involve explicitly the toroidal variable), the corresponding singular points are fixed points, such that we can associate invariant manifolds with them. Indeed, fractal structures have been observed in many different situations, including tokamak experiments [10,13,14]. An example of fractal distribution in toroidal plasmas is the magnetic footprint, a set of points at which the escaping chaotic orbits hit the tokamak wall. As a first approximation, charged particles follow magnetic field lines, hence the escaping field lines form preferential transport channels for charged plasma particles. Magnetic footprints then create hot spots in the tokamak wall with high concentrations of energy.

Many studies concerning nonlinear dynamics in tokamaks assume a collisionless plasma and that particles follow magnetic field lines [1]. A natural question that arises, therefore, is how particle motion and, in particular, particle collisions affect these fractal structures. To answer these questions we use a simple numerical model for particle motion, where collisions can be regarded as a noisy component in the magnetic field line equations.

In the late 90's, Balescu and collaborators have proposed a field line map (the *tokamap*) [15] that was not directly derived from magnetic field equations, but constructed to represent the global field line dynamics in a tokamak. It has been derived from a modified version of Wobig's generating function for a stellarator subjected to a localized perturbation [16]. The tokamap is designed to meet some desirable properties, like having an "impenetrable"

* Corresponding author.
E-mail address: viana@fisica.ufpr.br (R.L. Viana).

0375-9601/$ – see front matter
doi:10.1016/j.physleta.2011.10.025

magnetic axis, and admitting a realistic winding number profile, which in the model can be freely chosen. Furthermore, the tokamap is suitable for describing tokamaks with ergodic limiters, due to the existence of a chaotic field line region in the tokamak plasma edge.

Recently, it has been shown that noise can enhance the trapping of trajectories in scattering systems [17]. On the other hand, uncorrelated random perturbations can cause the escape of originally trapped orbits [18–20]. In this Letter, we present numerical evidence that the main effect of collisions is to disperse particles about the unstable manifold of the chaotic saddle that governs the magnetic field lines. We treat particle collisions as random perturbations acting on the particle trajectories, which follow themselves magnetic field lines. This idea dates back to the Monte Carlo codes for collisional diffusion equations [21].

The Letter is organized as follows. In Section 2 we make a brief description of the derivation of the magnetic field line mapping and introduce an extended version of this map with collisional effects. In Section 3 we show the fractal manifold structures that appear for the field lines dynamics, and discuss the time scale where these structures are robust. The results and analysis of the collisional tokamap are shown in Section 4. Our conclusions are presented in Section 5.

2. Model

Tokamaks are the most promising devices for the magnetic confinement of fusion plasmas. The stability of the plasma confinement in tokamaks is a problem in which the magnetic field line configuration plays a fundamental role – both by strongly influencing the transport that arises from fine scale turbulence and by being the leading order approximation to the particle flux since charged particles tend to follow the magnetic field lines. Magnetic field lines can be regarded as orbits of Hamiltonian systems of one-and-a-half degrees of freedom which are, provided the time-like coordinate is periodic, equivalent to two-dimensional conservative return maps [1,22]. Consequently we can employ two-dimensional Hamiltonian maps to describe the toroidal magnetic configurations of plasmas confined in tokamaks, a procedure which is particularly tailored for interpreting phenomena in the nonlinear dynamics framework.

Magnetic field lines in the tokamak can be written in the following Hamiltonian form

$$\frac{d\psi}{d\varphi} = -\frac{\partial H}{\partial \theta}, \qquad \frac{d\theta}{d\varphi} = \frac{\partial H}{\partial \psi}, \tag{1}$$

where the Hamiltonian H is the poloidal flux, θ and ψ represent the coordinate and momentum canonical variables, and the toroidal angle φ is a time-like variable. The Hamiltonian H can be divided into two parts: the unperturbed flux H_0 and the perturbed one H_1, resulting in $H = H_0 + \varepsilon H_1$ with

$$H_0(\psi) = \int \frac{d\psi}{q(\psi)}, \tag{2}$$

where $q(\psi)$ is known as the safety profile.

The parameter ε represents the relative strength of the magnetic perturbations, that can be described in terms of a Fourier series

$$H_1(\psi,\theta,\varphi) = \sum_{m,n} H_{m,n}(\psi)\cos(m\theta - n\varphi + \chi_{m,n}), \tag{3}$$

where m and n are the poloidal and toroidal mode numbers, and $\chi_{m,n}$ represent their phases. The magnetic perturbation is a 2π-periodic function of φ. Such periodicity allows for a simpler treatment of the system via stroboscopic maps.

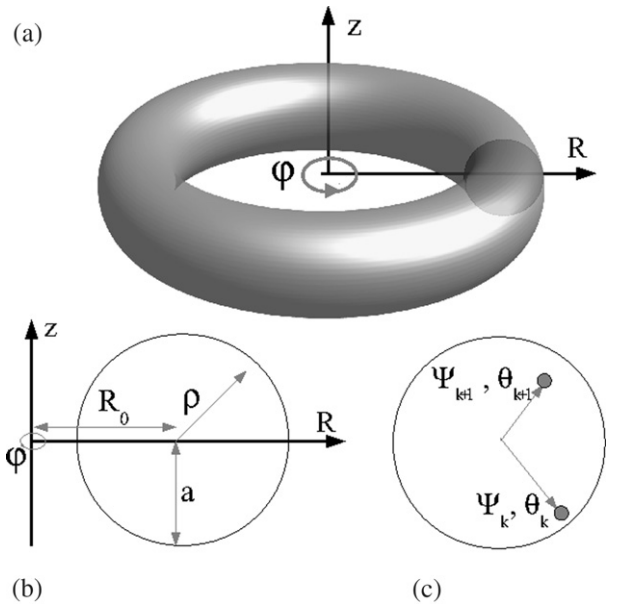

Fig. 1. Geometry and coordinates relevant for the tokamap. (a) Cylindrical coordinates (R,φ), and Z are used to describe a field line point in the tokamak torus. (b) Polar coordinates (ρ,θ) in a poloidal cross-section of the tokamak. (c) Two successive map points in a poloidal cross-section at constant azimuthal angle φ with $\psi \sim \rho^2$.

Thus, we introduce sections at $\varphi = \varphi_k = (2\pi/s)k$, with $(k = 0, \pm1, \pm2)$ and $s \geqslant 1$. If we take (ψ_k, θ_k) as the coordinates of the intersection points of the field lines with planes at $\varphi_k = \text{const.}$ (see Fig. 1), we can define a (forward) Poincaré map $(\psi_{k+1}, \theta_{k+1}) = \mathsf{T}(\psi_k, \theta_k)$.

Such construction allows us to create the following discrete system

$$\psi_{k+1} = \psi_k - \frac{\partial S(\psi_{k+1},\theta_k)}{\partial \theta_k} = \psi_k - \varepsilon \frac{\psi_{k+1}}{1+\psi_{k+1}}\sin(\theta_k), \tag{4}$$

$$\theta_{k+1} = \theta_k + \frac{2\pi}{q(\psi_{k+1})} + \frac{\partial S(\psi_{k+1},\theta_k)}{\partial \psi_{k+1}} = \psi_k + 2\pi\Omega(\psi_{k+1}) - \varepsilon\frac{1}{(1+\psi_{k+1})^2}\cos(\theta_k), \tag{5}$$

which can be regarded as canonical transformations from variables (ψ_k, θ_k) to $(\psi_{k+1}, \theta_{k+1})$ with the following generating function of the second kind

$$S(\psi_{k+1},\theta_k) = -\varepsilon\frac{\psi_{k+1}}{1+\psi_{k+1}}\cos(\theta_k). \tag{6}$$

The above map, proposed originally by Balescu et al. in [15], is called the *tokamap*. Although the tokamap was not directly derived from the magnetic field line equations, it meets some general and desirable properties, namely: (i) the avoidance of negative values of ψ, i.e. with $\psi_0 = 0$ implying $\psi_n \geqslant 0$ for all n; (ii) it is related to a realistic safety factor profile $q(\psi)$ (in contrast, e.g. with the Chirikov–Taylor standard map) [23].

In [24] it has been shown that from the Hamiltonian

$$H(\psi,\theta,\varphi) = \int \frac{d\psi}{q(\psi)} + \varepsilon\frac{\psi}{1+\psi}\cos(\theta)\sum_{s=-M}^{M}\cos(s\varphi), \tag{7}$$

with $M \to \infty$, one can obtain the following map:

$$\hat{\psi}_k = \psi_k - \frac{\varepsilon}{2}\frac{\hat{\psi}_k}{1+\hat{\psi}_k}\sin(\theta_k), \tag{8a}$$

$$\hat{\theta}_k = \theta_k - \frac{\varepsilon}{2}\frac{1}{(1+\hat{\psi}_k)^2}\cos(\theta_k),$$

$$\hat{\theta}_{k+1} = \hat{\theta}_k + \frac{2\pi}{q(\hat{\psi}_k)}, \tag{8b}$$

$$\psi_{k+1} = \hat{\psi}_k - \frac{\varepsilon}{2}\frac{\hat{\psi}_k}{1+\hat{\psi}_k}\sin(\theta_{k+1}), \tag{8c}$$

$$\theta_{k+1} = \hat{\theta}_{k+1} - \frac{\varepsilon}{2}\frac{1}{(1+\hat{\psi}_k)^2}\cos(\theta_{k+1}).$$

This map is called the *symmetric tokamap* and was already studied in [25]. The only equation that can be solved explicitly is Eq. (8a) with

$$\hat{\psi}_k = \frac{1}{2}\left[\sqrt{P^2(\psi_k,\theta_k)+4\psi_k} - P(\psi_k,\theta_k)\right], \tag{9}$$

where

$$P(\psi,\theta) = 1-\psi+\frac{\varepsilon}{2}\sin(\theta). \tag{10}$$

The other equations are numerically solved with the Newton method.

The symmetric tokamap can be inverted by making $\varepsilon \to -\varepsilon$ and $\Omega \to -\Omega$, generating the *backward tokamap*. Here, we choose to use the non-monotonic safety factor profile

$$q(\psi) = \frac{q_m}{1-a(\psi-\psi_m)^2}, \tag{11}$$

where $a = (1-q_m/q_0)/\psi_m^2$ and ψ_m is a minimum of the safety factor profile, given by

$$\psi_m = \left(1+\sqrt{\frac{1-q_m/q_1}{1-q_m/q_0}}\right)^{-1}, \tag{12}$$

with $q_0 = q(0) = 3$ and $q_1 = q(1) = 6$. This mapping is the so-called *revtokamap* [25].

Non-monotonic safety factor profiles in tokamaks can result from noninductive current drive methods like neutral beam injection [26]. The combination of Ohmic heating and current drive generate configurations with enhanced magnetic reversed shear and highly peaked density and pressure profiles. These discharges present reduction of the plasma transport, through the formation of a transport barrier, i.e., a region where both the electron and ion diffusivities are greatly reduced around the shearless position [27].

As a first approximation, one can consider that charged particles follow magnetic field lines. This, however, might not be accurate for situations where collisional effects become important. In order to address these cases, we now introduce a collisional term to the tokamap. In Refs. [28,29], a model for the heat transport in a chaotic magnetic field region was proposed. In that model, chaotic behavior is provided by the Chirikov–Taylor map dynamics, while the heat flow is represented by adding a random displacement of gyro-radius, ρ. Based on the same concept, collisional effects can be included in the tokamap by adding, with a probability P, a displacement ρ

$$(\psi_{k+1},\theta_{k+1}) = \mathsf{T}_f(\psi_k,\theta_k) + M^P(\rho), \tag{13}$$

where

$$M^P_\psi(\rho) = \rho\sin\phi, \qquad M^P_\theta(\rho) = \rho\cos\phi, \tag{14}$$

with $0 < \rho \leqslant \rho_m$. Here P is the collision probability from a given distribution function and ϕ is the angle, where $-\pi/2 < \phi < \pi/2$.

The inclusion of collisions in the tokamap leads to a stroboscopic map with an additional term that can be regarded as a noisy component, representing the collisional effect on the field lines. With this new term, the map becomes non-autonomous, that is, the map fully depends on the snapshot (i.e. the corresponding value of k) taken. Also, after this inclusion the map is no longer symplectic.

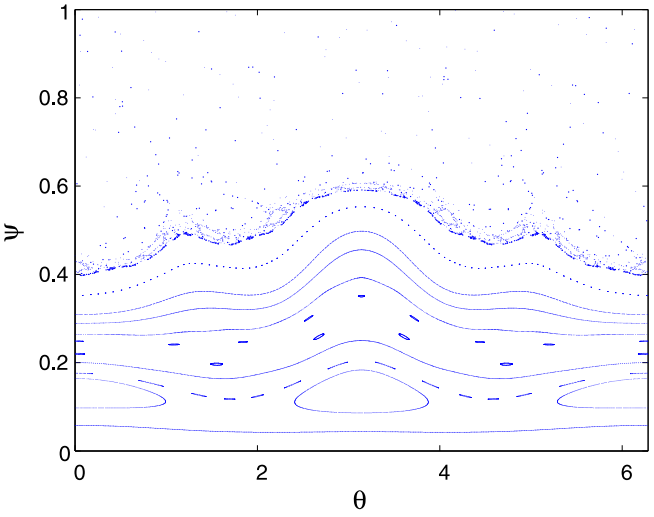

Fig. 2. (Color online.) Poincaré section of the Revtokamap with $\varepsilon = 6/2\pi$.

3. Magnetic field line dynamics

We show in Fig. 2 the Poincaré section of field lines obtained by iterating the forward tokamap with $\varepsilon = 6/2\pi$. The plot is shown in the (ψ,θ)-plane. As pointed out in Ref. [25], the phase space of Fig. 2 can be divided into two main regions: the laminar and the chaotic zones. The chaotic zone is formed at the plasma edge, while the laminar zone occupies the inner region of the Poincaré plot. Field lines with initial positions inside the chaotic region can reach the wall at $\psi = 1$ and, hence, escape the tokamak.

Because of the escaping field lines, the system can be viewed as a chaotic scattering phenomenon [33]. Indeed, the dynamics of magnetic field lines in tokamaks is frequently recognized as a chaotic scattering process [25,30,7]. Chaotic scattering is due to the presence of a non-attracting invariant set called the *chaotic saddle*, which we denote by Σ. Take, for example, an unstable periodic orbit inside the chaotic sea. The stable manifold, $W^S(\Sigma)$, of this point is formed by the set of points that reach the periodic orbit asymptotically *forward* in time, while the unstable manifold, $W^U(\Sigma)$, is a set of points that reach the periodic orbit *backward* in time. The chaotic saddle is a nonattracting dynamical invariant set formed by the homoclinic and heteroclinic intersections of the stable and unstable manifolds of all the (infinite) unstable periodic orbits embedded in the chaotic region [8]. These sets are invariant in the sense that their points map each other and, therefore, remain there forever.

Physically it is important to trace out the invariant manifolds and their associated chaotic saddle. For instance, it is through the unstable manifold that the magnetic field lines escape, forming the so-called *escape channels*. The stable manifold, on the other hand, highlights the initial position of field lines with longer connection lengths. The connection length is the number of toroidal turns it takes for a field line, originating from a given initial condition, located at the Poincaré section, to reach the tokamak wall. The connection length is thus a rough estimate of the escape time for a particle in the chaotic region to hit the tokamak wall. Thus, the chaotic saddle and its manifolds act as the dynamical skeleton underlying the chaotic behavior of the system, and its topological properties are similar to the Smale horseshoe [12].

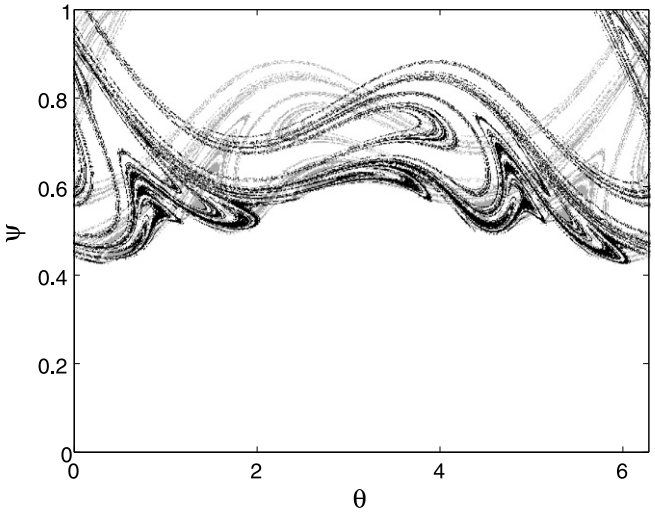

Fig. 3. Unstable (black filaments) and stable (gray filaments) manifolds of a fixed point in the chaotic region of the Poincaré section of Fig. 2.

Fig. 3 shows a numerical approximation of the unstable (black curves) and stable (gray curves) manifolds of a hyperbolic point embedded in a chaotic region of the field line map obtained in the previous section. The intersection of these sets form the chaotic saddle. We can see from Fig. 3 that the manifolds are convoluted sets, with filaments having a very intricate distribution. Geometrically, these structures form a fractal set, and we computed their box-counting dimension as $D = 1.75 \pm 0.04$. We have also calculated the Lyapunov exponent along the unstable direction that resulted in $\lambda = 0.286 \pm 0.02$. In the following, we explain the method that was used to compute the invariant sets shown in Fig. 3, as well as their dynamical properties.

There are different numerical techniques that can be used to obtain the invariant sets. In this work, we choose to use the *sprinkler method* [31]. The sprinkler method consists on taking a fine mesh (here we use 1000×1000 points) of initial positions in the chaotic region of interest, and iterating them until the corresponding orbits reach the tokamaks wall (at $\psi = 1$). The number of iterations necessary for each trajectory to reach the wall is called its *escape time*, denoted as t_{esc}. The initial positions that yield larger values of t_{esc} trace out the stable manifold of the chaotic saddle. To obtain the unstable manifold, we follow the same procedure using the backward-iterated tokamap.

On using the same numerical results obtained from the sprinkler method, we can also plot the escape basin, shown in Fig. 4. In the escape basin, each initial position is marked with a color code indicating its escape time – for larger values of t_{esc}, the corresponding pixel is lighter, while for fast escaping trajectories, the pixel is darker. The initial conditions which generate orbits that never escape, are represented by blank areas. From Fig. 4 we can see that the boundaries between regions with different values of the escape time trace out the stable manifold.

This is expected, since the intrinsic principle behind the sprinkler method is that long-lasting orbits of the map are located at the vicinity of the stable manifold. The method requires that all n_0 initial conditions we choose are uniformly distributed in a compact set (i.e., a box C) that contains the chaotic saddle. After a time t, almost all of the n_0 trajectories will have left C. In fact, if we consider, as a first approximation, the system to be hyperbolic, the decay rate of trajectories in C follows [32]

$$n(t) = n_0 \exp(t/\tau), \tag{15}$$

where $n(t)$ is the number of trajectories still in C at time t, and $1/\tau$ is the decay constant (inverse of mean lifetime). Fig. 5(a)

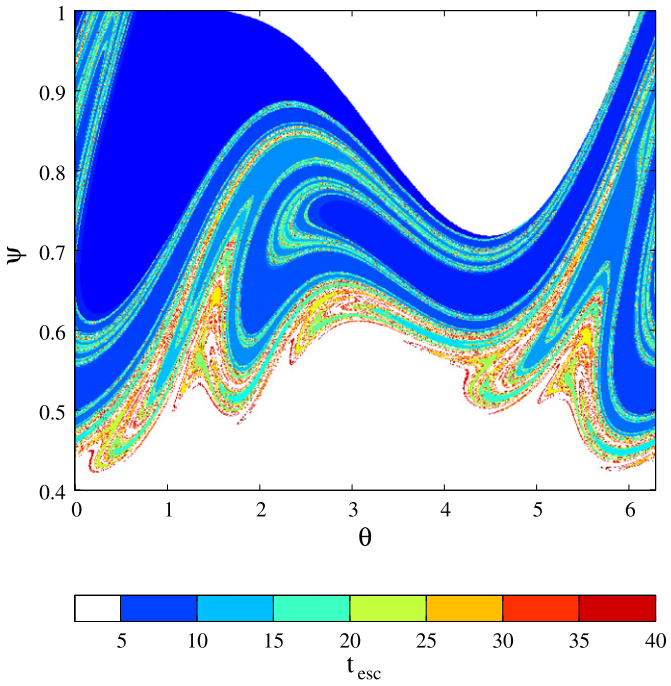

Fig. 4. (Color online.) Escape time distribution for the Revtokamap without collisions.

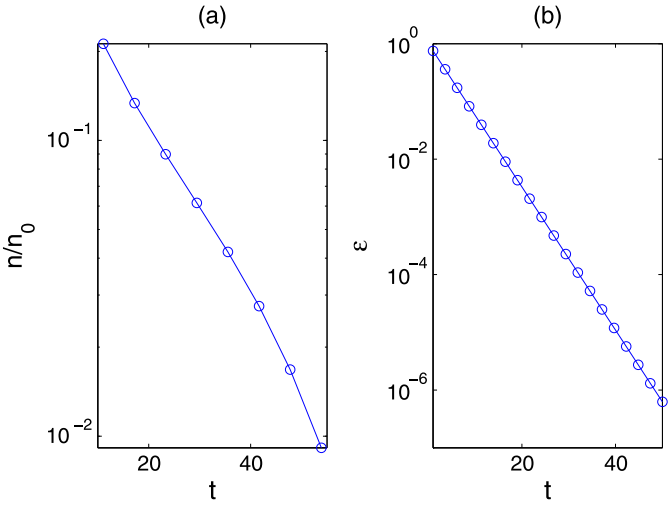

Fig. 5. (Color online.) (a) Number of map points in C with time and (b) width of initial conditions lying along the stable manifold.

shows the fraction of trajectories that remain in C as a function of time (here we consider C to be the region between the tokamak's wall and the last barrier of periodic islands). It turns out that the fraction of trajectories that remain in C actually follows Eq. (15), with a mean lifetime of $\tau = 14.5 \pm 1.0$.

It is worth mentioning that Eq. (15) is strictly valid only for hyperbolic chaotic systems. In the Poincaré plot shown in Fig. 2, we observe KAM tori separating the laminar from the chaotic zone. These tori are a source of non-hyperbolic dynamics – close to it there is stickiness of trajectories that leads to a power-law decay of the number of orbits remaining in C, instead of the exponential one [33]. Further from this boundary, however, the decay is exponential, as shown in Fig. 5. Thus, the escape of chaotic magnetic field lines in this case can still be described, in a good approximation, as a fully hyperbolic system.

It is important to remark that, for initial points close to the chaotic saddle, only a few iterates are enough for field lines to

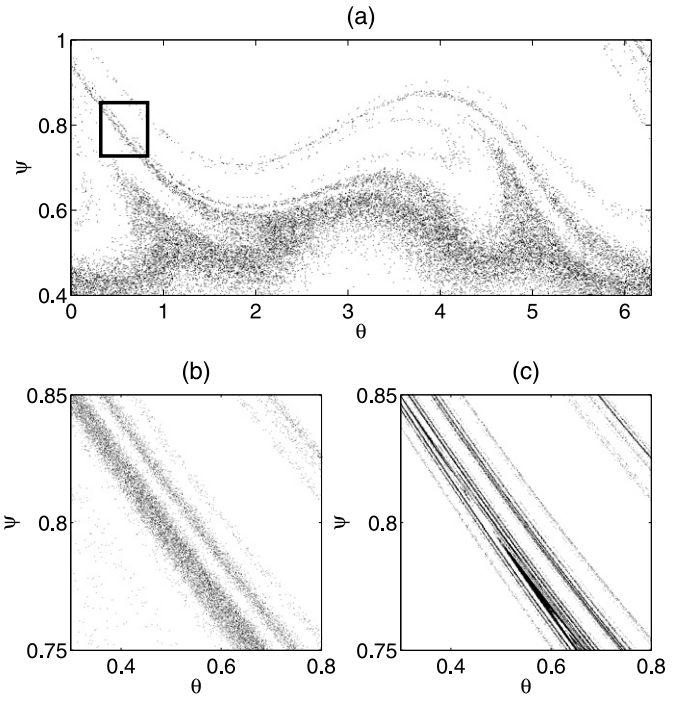

Fig. 6. (a) Ensemble of particles that trace out the unstable manifold for the tokamap with $\rho = 10^{-3}$ and $P = 1$. (b) Detail of (a). (c) The same region of (b) for the *collisionless* tokamap.

escape to the tokamak wall. After a finite time t, the n_t trajectories still inside C will have initial conditions lying in thin filaments along the stable manifold. The widths of these filaments can be estimated by [31]

$$\epsilon = \exp(-t\lambda), \tag{16}$$

where λ is the Lyapunov exponent along the unstable direction. For $t \to \infty$, the filament width $\epsilon \to 0$ and the initial positions lie in a Cantor-like structure, akin to that occurring in the invariant set of the Smale horseshoe [12]. The time-scale of real systems, however, is finite. On regarding this limitation, we now discuss how the above structures are affected when realistic plasma parameters are considered.

There are cases, depending on the plasma temperature and density, where the collision time is larger than the mean lifetime τ. In such situations, one can assume that the plasma particles follow field lines, and escape through the unstable manifold of the hyperbolic points. This is true for the lower density plasma condition. Collisions become important, however, when the plasma density is higher. For such cases, the collision time is smaller than the mean lifetime of field lines, meaning that the particles will have several collisions before escaping through the tokamaks wall. To address these cases, we add a collisional effect to the tokamap by including a noisy term in the field line mapping.

4. Collisional tokamap

In Fig. 6 we plot points that trace out the unstable manifold for the collisional tokamap with $P = 1$ and $\rho_m = 10^{-3}$. The main effect of the collisional term is that particles no longer trace out the unstable manifold $W^S(\Sigma)$ exactly, rather they disperse about it. As the collisional displacement, ρ_m, gets larger, the dispersion about $W^S(\Sigma)$ increases.

In order to describe this behavior quantitatively, we calculate the dispersion D_{S_1,S_2} of the set S_1 about the set S_2, where S_1 and S_2 are the sets of points that trace out the unstable manifold for the collisional and the collisionless tokamap, respectively. In [34] D_{S_1,S_2} is defined as the average of the distances $d(x, S_2)$ between the points $x \in S_1$ and the set S_2

$$D_{S_1,S_2} = \langle d(x, S_2) \rangle_{x \in S_1}, \tag{17}$$

where $d(x, S_2) = \min\{d(x, y), y \in S_2\}$.

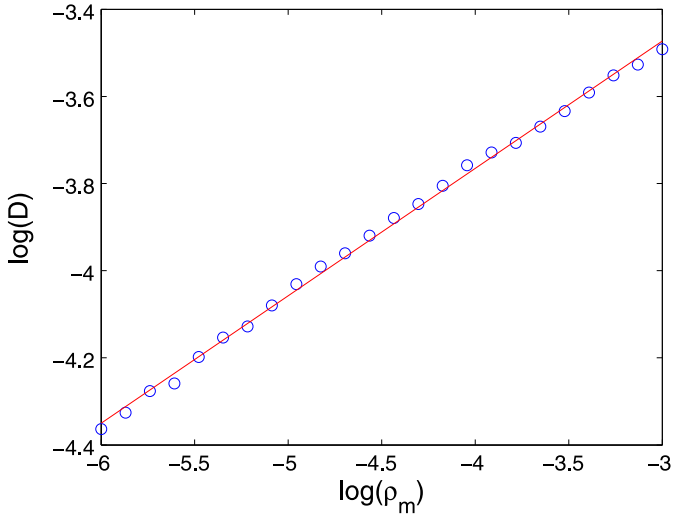

Fig. 7. (Color online.) Dispersion D as a function of the displacement parameter ρ_m.

Fig. 7 shows the variation of the dispersion D_{S_1,S_2} as a function of different values of the displacement parameter, ρ_m, yielding a power-law description. Numerical fitting gives us the power-law dependence:

$$D_{S_1,S_2}(\rho_m) = \rho_m^{\alpha}, \tag{18}$$

with $\alpha = 0.30 \pm 0.05$.

We now qualitatively discuss the dependence of the constant α on dynamical properties of the system. Suppose we take a small set of initial conditions, S_1, and follow the distribution of the corresponding orbit points with time. This distribution can be viewed as a droplet in a flow converging towards the unstable manifold [33]. The width ϵ of S_1 will change due to two different mechanisms: it will broaden due to collisions and contract along the stable manifold due to the presence of the chaotic saddle. The overall effect is that the droplet will converge to a narrow strip centered at unstable manifold, but not up to infinite precision. Collisions then have a diffusive effect that is visible only in small scales.

In Fig. 8 we show the evolution of a set of initial positions for the collisional tokamap (in red) and for the collisionless tokamap (in blue). The distribution S_1 traces out the unstable manifold, but there is also a spreading due to collisions. We also observe that, for the collisional case, the distribution covers the long filaments of the unstable manifold much faster than for the non-collisional case previously discussed.

To formulate this behavior, let us assume that the spreading effect over the filaments can be described by $(\epsilon_k^2 + 2Dt)^{1/2}$, where D is the diffusion coefficient of the collisional effect [33]. Likewise, the contraction factor is represented by $\exp(-\lambda t)$, where λ is the Lyapunov coefficient along the stable direction. The time evolution of the filament widths then reads

$$\epsilon_{k+1} = \left(\epsilon_k^2 + 2Dt\right)^{1/2} e^{-\lambda t}. \tag{19}$$

5. Conclusions

Plasmas confined in tokamaks with non-symmetric perturbations are surrounded by a chaotic layer of magnetic field lines that

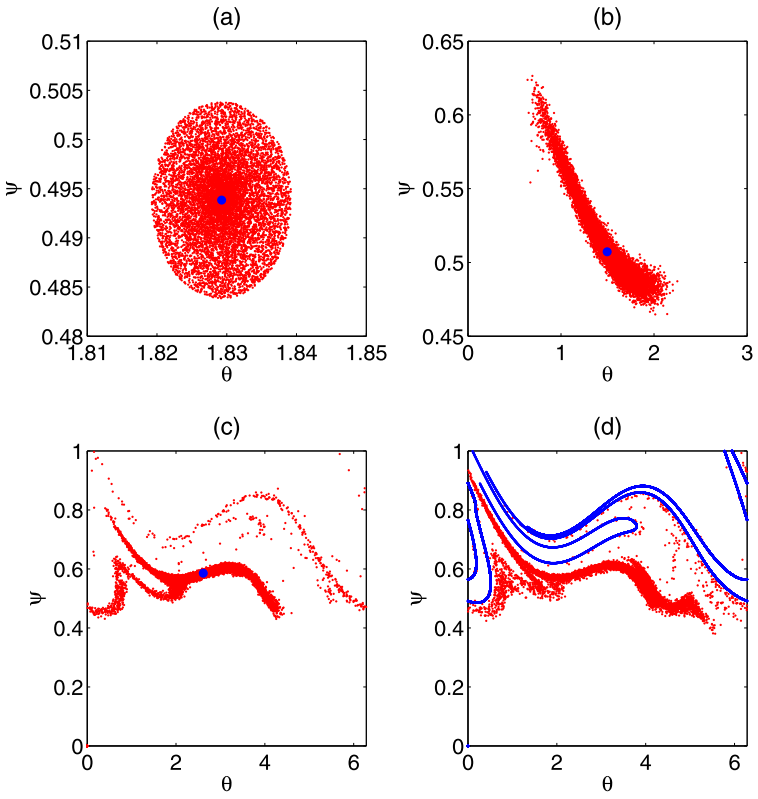

Fig. 8. (Color online.) Evolution of a set of initial positions for (a) $k = 2$, (b) $k = 10$, (c) $k = 20$ and (d) $k = 256$, with $\rho = 10^{-2}$ and $P = 1$. The red dots correspond to the distribution of the collisional tokamap and the blue dots are the distribution of magnetic field (collisionless tokamap).

guide charged particles to the wall. Moreover, the particles are deposited on the wall following a fractal distribution attributed to the field lines chaotic saddle in the chaotic layer surrounding the plasma. We use the tokamap, an analytical two-dimensional symplectic mapping, to obtain this chaotic saddle and the resultant fractal field lines escape to the wall. This is expected to explain the particle escape for low density plasma at the plasma edge. However, when the plasma density is higher the collision time is smaller than the mean lifetime of field lines, meaning that the particles may experience several collisions before escaping to the tokamak wall.

To investigate the influence of the collisions on the predicted particle escape distribution, we added a collisional term to the tokamap, assuming that collisions can be regarded as a noisy component. Within this procedure we found that the main effect of the collisional term is that particles no longer trace out the unstable manifold exactly, rather they disperse about it.

Furthermore, in order to describe this behavior quantitatively, we studied the dispersion of a set of points that trace out the unstable manifold for the collisional tokamap. We found that this dispersion yields a power-law description in terms of the displacement parameter. Moreover, we also discussed qualitatively the dependence of the power-law exponent on the dynamical properties of the system. Namely, we shown how a small set of initial conditions converges towards the unstable manifold of a hyperbolic point embedded in the chaotic region, forming highly convoluted filaments. We found that the filament widths changed due to two different mechanisms: the filaments broad out due to noise and contract along the stable manifold due to the presence of the chaotic saddle. The overall effect is that the droplet will converge to the unstable manifold, but not up to infinite precision. Collisions then have a diffusive effect that is visible only in small scales.

Generally, the average collision time depends on the plasma temperature and density and can be considered as a time parameter that measures whether the chaotic sets are robust or not. If the mean escape time of the field lines is larger than the particle collisional time, then the fractal structures can be considered robust. Physically, this means that the majority of particles escape through the unstable manifold before suffering a single collision. However, if the mean time between particle collisions is smaller than the mean escape time of field lines, the particles will experience several collisions before escaping to the tokamak wall. In this case of small collision time, our result suggests a mechanism to explain why particle collisions do not destroy the fractal structures (like magnetic footprints) observed in divertor plates due to escaping tokamak particles.

Acknowledgements

This work was made possible by partial financial support of CNPq, CAPES, FAPESP, Fundação Araucária, and RNF–CNEN (Brazilian Fusion Network).

References

[1] P.J. Morrison, Phys. Plasmas 7 (2000) 2279.
[2] I.L. Caldas, R.L. Viana, M.S.T. Araujo, A. Vannucci, E.C. da Silva, K. Ullmann, M.V.A.P. Heller, Braz. J. Phys. 32 (2002) 980.
[3] Ph. Ghendrih, M. Bécoulet, L. Colas, A. Grosman, R. Guirlet, J. Gunn, T. Loarer, A. Azéroual, V. Basiuk, B. Beaumont, A. Bécoulet, P. Beyer, S. Brémond, J. Bucalossi, H. Capes, Y. Corre, L. Costanzo, C. De Michelis, P. Devynck, S. Féron, C. Friant, X. Garbet, R. Giannella, C. Grisolia, W. Hess, J. Hogan, L. Ladurelle, F. Laugier, G. Martin, M. Mattioli, B. Meslin, P. Monier-Garbet, D. Moulin, F. Nguyen, J.-Y. Pascal, A.-L. Pecquet, B. Pégourié, R. Reichle, F. Saint-Laurent, J.-C. Vallet, M. Zabiégo, Tore Supra Team, Nucl. Fusion 42 (2002) 1221.
[4] W. Engelhardt, W. Feneberg, J. Nucl. Mat. 76–77 (1978) 556.
[5] C.J.A. Pires, E.A.O. Saettone, M.Y. Kucinski, A. Vannucci, R.L. Viana, Plas. Phys. Contr. Fusion 47 (2005) 1609.
[6] K.H. Finken (Ed.), Special Issue on the Dynamic Ergodic Divertor, Fusion Eng. Design 37 (1997) 335.

[7] E.C. da Silva, I.L. Caldas, R.L. Viana, M.A.F. Sanjuan, Phys. Plasmas 9 (2002) 4917.
[8] T. Kapitaniak, Y.-C. Lai, C. Grebogi, Phys. Lett. A 259 (1999) 445.
[9] E.C. da Silva, M. Roberto, J.S.E. Portela, I.L. Caldas, R.L. Viana, Nucl. Fusion 46 (2006) S192.
[10] A. Wingen, M. Jakubowski, K.H. Spatschek, S. Abdullaev, K.H. Finken, M. Lehnen, TEXTOR-team, Phys. Plasmas 14 (2007) 042502.
[11] R.L. Viana, E.C. da Silva, T. Kroetz, I.L. Caldas, M. Roberto, M.A. Sanjuán, Phil. Trans. Royal Soc. A 369 (2011) 371.
[12] J. Aguirre, R.L. Viana, M.A.F. Sanjuán, Rev. Mod. Phys. 81 (2009) 333.
[13] M.W. Jakubowski, A. Wingen, S.S. Abdullaev, K.H. Finken, M. Lehnen, K.H. Spatschek, R.C. Wolf, J. Nucl. Mat. 363–365 (2007) 371.
[14] T.E. Evans, R.A. Moyer, P. Monat, Phys. Plasmas 9 (2002) 4957.
[15] R. Balescu, M. Vlad, F. Spineanu, Phys. Rev. E 58 (1998) 951.
[16] H. Wobig, Z. Naturforsch. 42a (1987) 1054.
[17] E.G. Altmann, A. Endler, Phys. Rev. Lett. 105 (2010) 244102.
[18] J.M. Seoane, L. Huang, M.A.F. Sanjuán, Y.-C. Lai, Phys. Rev. E 79 (2009) 047202.
[19] C.S. Rodrigues, A.P.S. de Moura, C. Grebogi, Phys. Rev. E 82 (2010) 026211.
[20] C.S. Rodrigues, C. Grebogi, A.P.S. de Moura, Phys. Rev. E 82 (2010) 046217.
[21] M.H. Kalos, P.A. Whitlock, Monte Carlo Methods, Wiley–Blackwell, 2008.
[22] S.S. Abdullaev, Construction of Mappings for Hamiltonian Systems and Their Applications, Lecture Notes in Physics, vol. 691, Springer, Berlin, 2006.
[23] J.S.E. Portela, I.L. Caldas, R.L. Viana, Eur. Phys. J. Special Topics 165 (2008) 195.
[24] S.S. Abdullaev, Nucl. Fusion 44 (2004) S12.
[25] A. Wingen, K.H. Spatschek, S. Abdullaev, Contrib. Plasma Phys. 45 (2005) 500.
[26] T. Kroetz, M. Roberto, E.C. da Silva, I.L. Caldas, R.L. Viana, Phys. Plasmas 15 (2008) 092310.
[27] F.A. Marcus, T. Kroetz, M. Roberto, I.L. Caldas, E.C. da Silva, R.L. Viana, Z.O. Guimarães-Filho, Nucl. Fusion 48 (2008) 024018.
[28] J.M. Rax, R.B. White, Phys. Rev. Lett. 68 (1992) 1523.
[29] P. Beaufume, M.A. Dubois, M.S. Mohamed Benkadda, Phys. Lett. A 147 (1990) 87.
[30] S.S. Abdullaev, Th. Eich, K.H. Finken, Phys. Plasmas 8 (2001) 2739.
[31] G.-H. Hsu, E. Ott, C. Grebogi, Phys. Lett. A 127 (1988) 199.
[32] H. Kantz, P. Grassberger, Physica D 17 (1985) 75.
[33] E. Ott, T. Tel, Chaos 3 (1993) 417.
[34] R.D. Vilela, A.P.S. de Moura, C. Grebogi, Phys. Rev. E 73 (2006) 026302.